1   **Investigation of the functional relationship between antecedent rainfall and the probability**

2   **of debris flow occurrence in Jiangjia Gully, China**

3   Shaojie Zhang[1], Xiaohu Lei[1,4], Hongjuan Yang[1], Kaiheng Hu[1], Juan Ma[2], Dunlong Liu[3], Fanqiang Wei[4]

4   1. State Key Laboratory of Mountain Hazards and Engineering Safety, Institute of Mountain Hazards and

5   Environment, Chinese Academy of Sciences, Chengdu 610041, China

6   2.China Institute for Geo-Environment Monitoring, Beijing, 100081

7   3.College of Software Engineering, Chengdu University of Information and Technology, Chengdu, 610225, China

8   4.Chongqing Institute of Green and Intelligent Technology, Chinese Academy of Sciences, Chongqing 400714,

9   China

10   Correspondence to: Shaojie Zhang, E-mail: sj-zhang@imde.ac.cn; Kaiheng Hu, E-mail: khhu@imde.ac.cn

11   **Abstract**

12   A larger antecedent effective precipitation (AEP) indicates a higher probability of a debris flow

13   (P_{df}) being triggered by subsequent rainfall. Scientific topics surrounding this qualitative conclusion

14   that can be raised, including what kinds of variation rules do they follow, and whether there is a

15   boundary limit. To answer these questions, Jiangjia Gully in Dongchuan, Yunnan province, China,

16   is chosen as the study area, and a numerical calculation, rainfall scenario simulation, and Monte

17   Carlo integration method have been used to calculate the occurrence probability of debris flow under

18   different AEP conditions and derive the functional relationship between P_{df} and AEP. The

19   relationship between P_{df} and AEP can be quantified by a piecewise function. P_{df} is equal to 15.88%

20   even AEP reaches 85 mm indicating that debris flow in nature has an extremely small probability

21   compared to the rainfall frequency. Data from 1094 rainfall events and 37 historical debris flow

events are collected to verify the reasonability of the functional relationship. The results indicate

that the piecewise function are highly correlated with the observation results. Our study confirms

the correctness of the qualitative description of the relationship between AEP and P_{df}, clarifies that

debris flow is a small probability event compared to rainfall frequency, and quantitatively reveals

the evolution law of debris flow occurrence probability with AEP, which can provide a clear

reference for the early warning of debris flows.

Keywords: Debris flow, antecedent effective rainfall, Dens-ID, Monte Carlo method

1 Introductions

The antecedent effective precipitation (AEP) likes a Trojan horse lurking inside a loose soil

mass, which can cooperate with subsequent rainfall at any time to trigger debris flow in a debris-

flow gully. The AEP is equivalent to the precipitation preserved in soil mass before the triggering

rainfall process; it represents the saturation degree of loose soil mass (Segoni et al., 2018a;

Leonarduzz and Molnar, 2020). Therefore, the soil moisture that has accumulated from antecedent

rainfall since the beginning of a rainfall season has a significant influence on how new storm rainfall

interacts with the loose soil mass within a gully (Fiorillo and Wilson, 2004; Long et al., 2020). The

increase in AEP can decrease the shear strength of a loose solid material provided by shallow

landslides or channel erosion (Papa, et al., 2013; Senthilkumar et al., 2017; Liu et al., 2020), as a

consequence, the supply rate of solid material resources can be significantly enhanced in the

subsequent rainfall process (Wei et al., 2008; Bennett et al., 2014; Zhang et al., 2020). Additionally,

increased AEP and moisture content have been shown to enhance rainfall-induced surface runoff in

a variety of environments (Tisdall, 1951; Luk, 1985; Le Bissonnais et al., 1995; Castillo et al., 2003;

44   Jones et al., 2017; Hirschberg et al., 2021). Thus, AEP plays an important role in the formation of

45   debris flows (Hong et al., 2018).

46   Rainfall thresholds represent the difficulty degree of debris flow triggered by rainfall (Marra

47   et al., 2017). Investigations including the influence of AEP on the rainfall threshold can be helpful

48   to examining the relationship between AEP and debris flow occurrence. Currently, the relationship

49   between the AEP and rainfall threshold indicates that there is a negative correlation between the

50   AEP and rainfall conditions that trigger debris flows (Huang, 2013). AEP also represents the

51   saturation degree of loose soil mass (Zhao et al., 2019a; Abraham et al., 2021), and integrating soil

52   moisture with rainfall thresholds has been proven effective in improving prediction performance

53   (Segoni et al., 2018a; Zhao et al., 2019b; Abraham et al., 2020). Scholars also have attempted to

54   analyze the influence of antecedent soil moisture on the rainfall threshold triggering debris flow

55   (Cui et al., 2007; Hu et al., 2015), and there is still a negative correlation between antecedent soil

56   moisture and triggering rainfall conditions (Chen et al., 2017) just like the relationship between AEP

57   and rainfall threshold. The above investigations show that increasing in AEP can significantly

58   decrease the rainfall conditions for triggering a debris flow, which in turn means that debris flow is

59   more likely to occur. Generally, the qualitative description of 'the greater the AEP, the higher the

60   probability (P_{df}) of subsequent rainfall triggering the debris flow (De Vita et al., 2000; Bel et al.,

61   2017)' has gradually become a consensus. Therefore, discovering a specific function to describe this

62   qualitative description is helpful to further demonstrating the above consensus, revealing a certain

63   evolutionary law of debris flow with rainfall in nature.

64   To quantify the evolution law of P_{df} with the changing AEP, a numerical model denoted as the

65   Dens-ID can correlate the rainfall parameters (I and D) with the debris flow density (Zhang et al.,

2020; Long et al., 2020; Zhang et al., 2023), and it has been used to construct the rainfall intensity-duration (ID) threshold curves under different AEP conditions. The ID threshold curves with upper and lower bounds can delineate the closed region in the ID coordinate system, which represents the set of all rainfall conditions that can trigger debris flow at a certain AEP. Consequently, the probability of natural rainfall falling into a closed region is equivalent to P_{df}, which can then be calculated based on Monte Carlo integration. The next section introduces the basic information of study area including the rainfall and debris flow event data collected from the study area. The third section addresses how to establish the functional relationship between the AEP and Pdf using the Dens-ID and Monte Carlo integration method. Section 4, 5 and 6 discuss the results and state the conclusions of this study, respectively.

2 Study areas

The Jiangjia Gully (JJG) is a primary tributary of the Xiaojiang River, which is located in the Dongchuan District of Kunming City, Yunnan Province, China (Fig.1). As shown in Fig.1, JJG has a drainage area of 48.6 km^2 with elevations ranging from 1040to 3260 m. In this gully, the relative relief from the ridge to the valley reaches 500 m, and most of the slope gradient is greater than 25°. Slopes within JJG are covered by abundant loose soil with a thickness of more than ten meters. Shallow landslides are frequently triggered by intense rainfall processes in JJG, providing a large number of solid materials for debris flow (Yang et al., 2022). Before 1979, the Menqian and Duozhao gullies are the two main tributaries of JJG, accounting for 64.7% of the entire drainage area. The upstream areas of the two main tributaries are the initiation zones of the debris flows, and the channels of the upstream tributaries are narrow and V-shaped (Zhang et al., 2020). However, several check dams have been constructed in the Duozhao gully since 1979, which have significantly reduced debris flow activity in this sub-gully (Zeng et al., 2009). Currently, Menqian Gully with the area of 13.2 km^2 is the primary source area. The slope gradient of its both sides is very steep, e.g., the mean slope in Menqian Gully is 32° and the maximum slope can reach 70°.

Bedrock that mainly consists of slates formed in lower Proterozoic crops out in the unvegetated or sparsely vegetated lower part. The bedrock is fragmented and mostly disintegrates into clasts with the size more than 20 mm. The upper part of the bedrock is lain by soil mantles with thicknesses of 0.5–20 m, which are covered by grasses and shrubs, or are used for terrace farming. The soil mantle is poorly sorted and composed of particles from clay to boulder. The translational zone from the upper to the lower parts of the slope is prone to shallow landslides. Some landslides directly evolve into debris flows, while the others release sediment to the channel, which is mobilized by runoff in debris flow events (Yang et al., 2022).
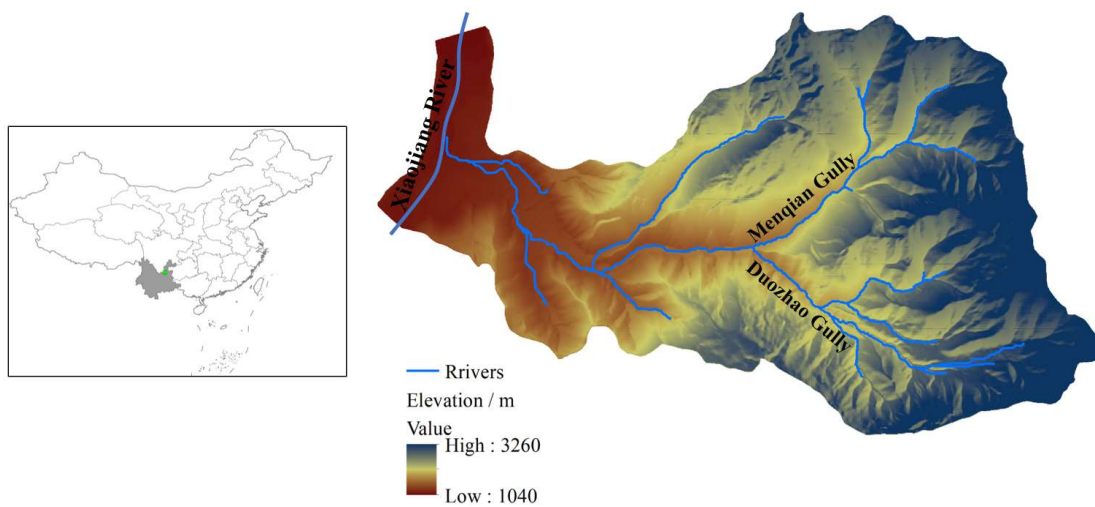
Fig.1 Location of JJG

Steep terrain provides a beneficial potential energy condition for transporting a large amount of loose solid materials from JJG to Xiaojiang River. Consequently, debris flows in JJG can be easily triggered by high-intensity rainstorm or long-duration rainfall processes (Zhang et al., 2020). The solid material necessary for a debris flow in a gully may be from shallow landslides (Iverson et al., 1997; Gabet and Mudd, 2006; Zhang et al., 2020; Long et al., 2020) or runoff-induced bed erosions (Berti and Simoni, 2005; Coe et al., 2008; Tang et al., 2020; Bernard and Gregoretti, 2021). In JJG, shallow landslides are the main sources for the solid material supply (Zhang et al., 2014; Liu et al., 2016; Yang et al., 2022), which is consistent with the assumptions of Dens-ID (Zhang et al., 2020). Thus, JJG is used as the study zone for deriving the function that describes the relationship between

110 AEP and P_{df}.

3 Methods and data

3.1 Dens-ID

113 Debris flow gullies characterized by a solid source supply from landslides are widely

114 distributed in southwest China (Zhang et al., 2014). For this type of debris flow gully, our previous

115 study proposed Dens-ID aiming at correlating debris-flow density to rainfall parameters based on

116 water-soil coupling mechanism (Zhang et al., 2020; Long et al., 2020). Den-ID assumes debris flow

117 to be a water-soil mixture, it contains three core simulating contents including hydrological

118 simulation, water-soil coupling to calculate the water-soil-mixture density, and correlating density

119 to rainfall parameters.

120 (1) Simulating hydrological process: the purpose is to provide parameters for estimating

121 rainfall-induced runoff and the supply volume of rainfall-induced loose solid materials. Based on

122 the digital elevation model (DEM) of a gully, Den-ID can simulate the rainfall-induced runoff and

123 water diffusion in the vertical direction within the soil mass. The rainfall infiltration border is

124 controlled by Equation 1.

$$-D(\theta)\frac{\partial \theta}{\partial z} + K(\theta) = I(t) \tag{1}$$

126 where θ is the soil water content; $D(\theta) = K(\theta)/(d\theta/d\psi)$, which represents the soil water

127 diffusivity; z is the soil depth, which is positive downwards along the soil depth as the topsoil is

128 taken as the origin point; $K(\theta)$ is the hydraulic conductivity; $I(t)$ is the rainfall intensity; and ψ is

129 the soil matrix suction. When the rainfall intensity is less than the surface infiltration capacity,

130 Equation 1 is used to represent this physical process; whereas the case of precipitation intensity

131 exceeding the infiltration capacity of topsoil means that the surface is saturated, and the excess

132   precipitation from the topsoil is converted into runoff. Therefore, the pressure infiltration of each

133   grid cell is not considered.

$$\frac{\partial \theta}{\partial t} = \frac{\partial}{\partial z}\left[D(\theta)\frac{\partial \theta}{\partial z}\right] - \frac{\partial K(\theta)}{\partial z} \tag{2}$$

135   Equation 2 is the Richard differential infiltration equation (Richards, 1931), which is used to

136   describe the water movement along the vertical direction within soil mass after precipitation

137   infiltrates into topsoil. Dens-ID uses the finite-difference method to solve Eqs. 1 and 2 and can

138   provide the runoff depth (denoted as $dw(i,t)$), soil water content, and soil matrix suction for each

139   grid cell. Dens-ID then calculates the runoff volume using runoff depth $dw(i, t)$ in Equation 3.

$$V_w(t) = \sum_{t=1}^{T} \sum_{i=1}^{n} S_g * dw(i,t) \tag{3}$$

141   where n represents the total number of grid cells that can generate runoff at time t, $V_w(t)$ represents

142   the total volume of runoff within a gully at time t, S_g represents the area of the grid cell generating

143   runoff, and T represents the total duration of a rainfall process.

144   (2) Calculating supply amount of loose solid materials and density of the water-soil mixture:

145   taking hydrological parameters such as soil water content and soil matrix suction as inputs, Dens-

146   ID uses Equations 4 and 5 to estimate the supply amount of rainfall-induced loose solid materials

147   within a gully. Equation 4 calculates safety factor F_s of each grid cell as a function of the matrix

148   suction and soil moisture. $F_s > 1$ indicates that the grid cell is stable and cannot supply solid material

149   to the gully, whereas a grid with $F_s < 1$ can provide solid material in the form of a shallow landslide.

$$F_s = \frac{\tan\varphi}{\tan\beta} + \frac{c + \psi \, ta \ (\varphi^b)}{\gamma_t d_s \cos\beta \sin\beta} \tag{4}$$

151   where F_s represents the safety factor of each grid cell, c is the soil cohesion force, φ is the internal

152   friction angle, φ^b is related to the matrix suction and is approximately equal to φ as the low matrix

153   suction is small, d_s is the soil depth, and ψ is the matrix suction which is a function of soil water

154   content and can be described by the Van Genuchten model (Van Genuchten, 1980).

155   Equation 4 is used to estimate the total volume of solid materials from all the unstable grid

156   cells during a rainfall process.

157
$$V_s(t) = \sum_{t=1}^{T} \sum_{j=1}^{m} S_g * ds(j,t) \tag{5}$$

158   where m represents the number of grid cells that can provide solid material at time t and $V_s(t)$ is the

159   total volume of solid material within a gully at time t. At time t, the density of the water-soil mixture

160   after full coupling between runoff and solid material can be calculated using Equation 6.

161
$$\rho_{mix}(t) = \frac{\rho_w V_w(t) + \rho_s V_s(t)}{V_{mix}(t)} \tag{6}$$

162   where $\rho_{mix}(t)$ is the density of the water-soil mixture, ρ_w is the water density, ρ_s is the density of

163   the soil particles, and $V_{mix}(t)$ is the volume of the water-soil mixture, which is the sum of $V_w(t)$

164   and $V_s(t)$. $V_w(t)$ and $V_s(t)$ are the key variables that can be derived using Eqs. 3 and 5.

165   (3) Correlating density to rainfall parameters including rainfall intensity and duration: after

166   firstly presetting the density of the water-soil mixture as ρ_{mix}, Dens-ID also needs to simulate many

167   rainfall scenarios including long durations with low-intensity rainfall and short durations with high-

168   intensity rainfall in order to obtain a sufficient number of [D_i, l_i]. Using each [D_i, I_i] as input, Dens-

169   ID then can calculate the density using Equation 6. If the calculated density is equal to ρ_{mix}, the [D_i,

170   I_i] combination is saved by Dens-ID. After Dens-ID completes the trial calculations, all combination

171   data of [D_i, I_i] that satisfy the constraints of the preset density (ρ_{mix}) can be collected as a dataset.

172   Each collected [D_i, I_i] within the dataset corresponds to the preset ρ_{mix}, accordingly, Dens-ID can

173   correlate rainfall parameters (D and I) to debris flow density (Long et al., 2020). Dens-ID can derive

174   ID threshold curves by fitting the selected [D_i, I_i] data, and each ID curve corresponds to a debris

175   flow density value (Zhang et al., 2020). As the density of debris flow in JJG varies in a specific

176   interval of 1.2–2.3g/cm³ (Zhang et al., 2014; Zhuang et al., 2015; Long et al., 2020), the threshold

177   curve that corresponds to the boundary value can form a closed area with the I- and D-axes in the

178   ID coordinate system. The case of monitoring or forecasting rainfall falling into this closed area

179   indicates that the rainfall condition may trigger debris flow. The verification results in JJG show

180   that Dens-ID can effectively describe the mechanism and process of debris flow formation, and its

181   prediction accuracy is approximately 80.5%, which is 27.7% higher than that of statistical models

182   (Zhang et al., 2020). Such a high prediction accuracy can further indicate that the closed area formed

183   by the derived ID curves has a very reasonable location and coverage in the ID coordinate system,

184   providing extremely reliable analytical data in this study.

185   **3.2 JJG data for model Dens-ID**

186   The JJG datasets for Dens-ID are terrain data, hydrological parameters, and soil mechanical

187   parameters. The DEM is the basal data for deriving other terrain data, including slope length,

188   gradient, and river channels; the spatial resolution of the DEM is 0.5 m, and a DEM with a grid size

189   of 10 m was generated using the resampling technology in ArcGIS. The hydrological parameters

190   are related to the soil types within JJG; the five key parameters are the saturated soil water content,

191   residual soil water content, the two parameters of soil water characteristic curve including *n* and *m*,

192   and the infiltration rate of topsoil. The soil mechanical parameters are the soil cohesion force and

193   internal friction angle obtained through direct shear tests on the soil samples. Detailed data are

194   available in Zhang et al. (2020) and Long et al. (2020).

195   **3.3 Historical rainfall and debris flow data**

196   Rainfall data for the rainy seasons between 2006 and 2020 have been collected from the JJG

197   observation station, and it is necessary to identify each rainfall process from the long-term rainfall

198   sequences. Inter-event time (IET) is defined as the minimum time interval between two consecutive

199   rainfall pulses (Adams et al., 1986). IET has a strong influence on the rainfall event starting and

200   ending times (Bel et al., 2017), and Peres et al. (2018) has identified that IET depends on whether

201   the mean daily potential evapotranspiration (MDPE) is larger than precipitation within the IET. The

202   long observation of evaporation within JJG showed that MDPE is about 4 mm; precipitation during

203   IET >0.5 mm is considered the end of a rainfall process. Under this standard, 1094 rainfall events

204   and 37 debris flow events have been identified during the sampling period. Detailed rainfall data

205   information can be found in "appendix 1-1094 rainfall and 37 debris flow data.xlsx". The AEP listed

206   in this appendix is considered the weighted sum of the rainfall periods before the occurrence of

207   debris flow (Long et al., 2020) and it can be calculated using Equation 7.

208    $$AEP = \sum_{i=1}^{n} K^n R_i \tag{7}$$

209   where AEP is the antecedent effective rainfall; K is the attenuation coefficient, which is equal to

210   0.78 based on the field test in JJG (Zhang et al., 2020); and n is the number of days preceding the

211   debris flow occurrence.

212   Based on the observed rainfall data, the 1094 AEPs are calculated using Equation 7 and listed

213   in Appendix 1. The AEP corresponding to each rainfall event varies from 0–88 mm. Taking this

214   variation range as a reference, the variation range of the AEP input in the Dens-ID model is set

215   between 10 and 85 mm. Since AEP in JJG ranges in 0-88 mm according to the measured rainfall

216   data, Dens-ID presets several AEP values including 10, 15, 20, 25, 30, 35, 40, 45, 50, 55, 60, 65, 70,

217   75, 80, 85. The cases of AEP=0 and AEP=5 mm are excluded, because the two cases represents such

218   a low initial rainfall condition that any ID curve cannot derived from Dens-ID. The purpose of

219   increasing AEP by an interval of size 5 is to get adequate ID curves, which will be helpful to

220   calculate P_{df} under different AEP conditions.

221   **3.4 Monte Carlo method for calculating the definite integral**

222   Because of the boundary of the debris-flow density in JJG (1.2–2.3g/cm³), Dens-ID produces

223   the corresponding upper and lower boundary curves under a specific AEP condition. The two

224   boundary curves can be described using the power function.

225
$$\begin{cases} f(D)_{up} = I_{up} = \alpha_1 D^{\beta_1} & D\epsilon[a_1, b_1] \\ f(D)_{low} = I_{low} = \alpha_2 D^{\beta_2} & D\epsilon[a_2, b_2] \end{cases} \tag{8}$$

226   These two threshold curves can delineate an enclosed area in the ID coordinate system, denoted

227   as W_{ID}. The independent variable (D) and dependent variable (I) in Equation 8 also form a closed

228   rectangular region in the ID coordinate system, denoted as R_{ID}. In the ID coordinate system, the

229   coverage of R_{ID} is larger than that of W_{ID}, as will be shown in detail in Section 4.1. Limited within

230   R_{ID}, any rainfall processes located in W_{ID} can trigger debris flow. If the probability of rainfall

231   process falling into the range of W_{ID} under random conditions is determined, the occurrence

232   probability of debris flow can be estimated. Many physical phenomena are stochastic in nature and

233   governed by stochastic partial differential equations with nondeterministic initial/boundary

234   conditions or integral equations (Peres and Cancelliere, 2014; Yan and Hong, 2014). Albert (1956)

235   proposed the Monte Carlo method for solving integral equations. This method is subsequently used

236   to estimate the peak flow and volume of debris flow (Donovan and Santi, 2017; Paola et al., 2017),

237   entrainment of the underlying bed sediment (Han et al., 2015), and risk assessment (Calvo and Savi,

238   2009; Li et al., 2021). The rainfall process is randomly selected within the R_{ID}, and the probability

239 of the chosen one falling into the W_{ID} can be determined using W_{ID}/R_{ID}. The physical meaning of

240 the Monte Carlo solving definite integral lies on calculating the area enclosed by the function curve

241 and horizontal axis. Therefore, the area of W_{ID} can be calculated by the difference in the definite

242 integral formula of the two equations in Equation 8.

243
$$W_{ID} = S_{up} - S_{low} = \int_{a1}^{b1} f(D)_{up} dD - \int_{a2}^{b2} f(D)_{low} dD \tag{9}$$

244 where S_{up} and S_{low} represent the area enclosed by the two threshold curves and the horizontal axis,

245 respectively, and a_1, b_1, a_2, and b_2 are the boundary values of D in the two curves. For the upper

246 boundary line (or lower boundary), if the probability distribution function of D between [a1, b1] is

247 p(D), Equation 10 can be derived by substituting p(D) into Equation 9.

248
$$\begin{cases} S_{up} = \int_{a_1}^{b_1} f(D)_{up} dD = \int_{a_1}^{b_1} \frac{f(D)_{up}}{p(D)} p(D) dD \approx \frac{1}{n} \sum_{k=1}^{n} \frac{f(D_i)_{up}}{p(D_i)} \\ S_{low} = \int_{a_2}^{b_2} f(D)_{low} dD = \int_{a_2}^{b_2} \frac{f(D)_{low}}{p(D)} p(D) dD \approx \frac{1}{n} \sum_{k=1}^{n} \frac{f(D_i)_{low}}{p(D_i)} \end{cases} \tag{10}$$

249
$$W_{ID} = \frac{1}{n} \sum_{k=1}^{n} \frac{f(D_i)_{up}}{p(D_i)} - \frac{1}{n} \sum_{k=1}^{n} \frac{f(D_i)_{low}}{p(D_i)} \tag{11}$$

250 where n represents the number of random samples drawn from the variation range of D, and $p(D_i)$

251 is the probability density distribution function of D in the interval $[a_1,b_1]$ or $[a_2,b_2]$. The key to

252 solving Equation 10 depends on sampling from p(D). The following steps are used to explain how

253 samples were taken using $p(D_i)$.

254 Step 1: Based on the probability density distribution function p(D), the cumulative probability

255 distribution function can be derived by cdf(D)$=\int_{-\infty}^{b} f(D) dD$;

256 Step 2: Assume that $U^{(i)}$ obeys a uniform distribution within [0,1], which can be randomly collected

257 from this interval and denoted as $U^{(i)} \sim U(0,1)$.

258 Step 3: Substitute $U^{(i)}$ into the inverse function of the cumulative probability distribution cdf(D) to

259 obtain random sample $D^{(i)}$, denoted by $D^{(i)} = cdf^{-1}(U^{(i)})$. Then, a dataset composed of n data

260 points of $D^{(i)}$ is obtained.

261   Step 4: W_{ID} can be calculated by substituting n data points of $D^{(i)}$ into Equation 10, and the P_{df}

262    $(P_{df} = \frac{R_{ID}}{W_{ID}})$ corresponding to a specific AEP is determined. P_{df} represents the probability that the

263   subsequent precipitation process may trigger debris flow for a certain AEP. Thus, the influence of

264   the AEP on the occurrence probability of debris flows can be quantified.

265   **3.5 Correlation analysis between numerical and observation results**

266   The relationship between the AEP-P_{df} fitted through the observational data is used as a

267   reference standard, and the correlation analysis method is used to verify the function of the AEP-P_{df}

268   derived by Dens-ID. Correlation analysis is used to study the degree of linear correlation between

269   variables, which is represented by correlation coefficient r:

270    $$r = \frac{\sum_{i=1}^{n}(x_i - \bar{x})(y_i - \bar{y})}{\sqrt{\sum_{i=1}^{n}(x_i - \bar{x})^2 \sum_{i=1}^{n}(y_i - \bar{y})^2}} \qquad (12)$$

271   where x represents the P_{df} derived from the observed data, y represents the P_{df} derived from Dens-

272   ID, $\bar{x}$ and $\bar{y}$ represent the averages, r represents the correlation coefficient, and n represents the

273   number of samples. $|r| \geq 0.8$ can be regarded as a high correlation between two variables; $0.5 \leq |r| < 0.8$

274   represents a moderate correlation; $0.3 \leq |r| < 0.5$ represents a low correlation; and $|r| < 0.3$ indicates the

275   degree of correlation between the two variables is weak and can be regarded as uncorrelated.

276   **4 Results**

277   **4.1 ID threshold curves and warning zone closed by the derived curves**

278   Dens-ID yields the upper and lower boundary lines of the ID threshold in each condition of a

279   preset AEP, and these two boundary lines are characterized by different debris flow density and

280   listed in Table 1. It can be seen from Table 1 that the maximum density corresponding to the ID

281   threshold curve cannot reach 2.2, when AEP is less than15 mm. A small AEP indicates the supply

282   rate of solid resources in JJG is far less than the runoff generation rate during a subsequent rainfall

283 process. In this situation, runoff is dominated in the water-soil coupling process yielding a water-

284 soil mixture with low density value.

285

Table 1 ID threshold curve database under different AEP

AEP (mm)	ID threshold curve function for JJG	
	1.2 g/cm^3	2.2 g/cm^3
10	$I_{1.2} = 19.85D^{-0.54}$ D∈[1, 269] ($R^2 = 0.991$)	$I_{1.8}=15.85D^{-0.48}$ D∈[1, 263] ($R^2=0.990$)
15	$I_{1.2}= 21.69D^{-0.55}$ D∈[1, 236] ($R^2=0.993$)	$I_{2.0}=16.10D^{-0.50}$ D∈[1, 229] ($R^2=0.995$)
20	$I_{1.2}=23.22D^{-0.58}$ D∈[1, 203] ($R^2=0.996$)	$I_{2.2}=17.20D^{-0.53}$ D∈[1, 192] ($R^2=0.995$)
25	$I_{1.2}=24.47D^{-0.60}$ D∈[1, 171] ($R^2=0.997$)	$I_{2.2}=16.92D^{-0.53}$ D∈[1, 160] ($R^2=0.998$)
30	$I_{1.2}=26.24D^{-0.64}$ D∈[1, 143] ($R^2=0.996$)	$I_{2.2}= 18.09D^{-0.57}$ D∈[1, 132] ($R^2=0.995$)
35	$I_{1.2}=35.47D^{-0.65}$ D∈[1, 123] ($R^2=0.958$)	$I_{2.2}= 19.55D^{-0.58}$ D∈[1, 112] ($R^2=0.985$)
40	$I_{1.2}= 40.59D^{-0.78}$ D∈[1, 103] ($R^2=0.966$)	$I_{2.2}= 22.15D^{-0.64}$ D∈[1, 92] ($R^2=0.984$)
45	$I_{1.2}= 41.12D^{-0.78}$ D∈[1, 83] ($R^2=0.932$)	$I_{2.2}= 23.19D^{-0.69}$ D∈[1, 72] ($R^2=0.981$)
50	$I_{1.2}=41.26D^{-0.86}$ D∈[1, 65] ($R^2=0.981$)	$I_{2.2}= 23.50D^{-0.74}$ D∈[1, 55] ($R^2=0.980$)
55	$I_{1.2}=38.63D^{-0.88}$ D∈[1, 53] ($R^2=0.950$)	$I_{2.2}= 23.31D^{-0.70}$ D∈[1, 42] ($R^2=0.932$)
60	$I_{1.2}= 31.49D^{-0.92}$ D∈[1, 40] ($R^2=0.992$)	$I_{2.2}= 20.73D^{-0.86}$ D∈[1, 30] ($R^2=0.977$)
65	$I_{1.2}= 29.14D^{-0.95}$ D∈[1, 32] ($R^2=0.957$)	$I_{2.2}= 18.10D^{-0.91}$ D∈[1, 22] ($R^2=0.893$)
70	$I_{1.2}= 23.05D^{-0.96}$ D∈[1, 25] ($R^2=0.998$)	$I_{2.2}= 13.04D^{-0.93}$ D∈[1, 15] ($R^2=0.995$)
75	$I_{1.2}= 21.13D^{-0.97}$ D∈[1, 22] ($R^2=0.994$)	$I_{2.2}=10.90D^{-0.95}$ D∈[1, 12] ($R^2=0.995$)
80	$I_{1.2}= 18.72D^{-0.98}$ D∈[1, 20] ($R^2=0.997$)	$I_{2.2}= 9.96D^{-0.95}$ D∈[1, 11] ($R^2=0.999$)
85	$I_{1.2}= 18.47D^{-0.99}$ D∈[1, 18] ($R^2=0.999$)	$I_{2.2}= 8.17D^{-0.95}$ D∈[1, 9] ($R^2=0.999$)

286 Under the condition of AEP < 10 mm, Dens-ID cannot derive the threshold curve

287 corresponding to even the minimum density value of 1.2 g/cm^3, which indicates that the subsequent

288 rainfall can hardly trigger debris flow JJG. Table 1 also shows that the AEP ranging from 10 to 85

289 mm can significantly affect the ID threshold curve, because the parameters including α and β

290 regularly respond to the change in AEP.
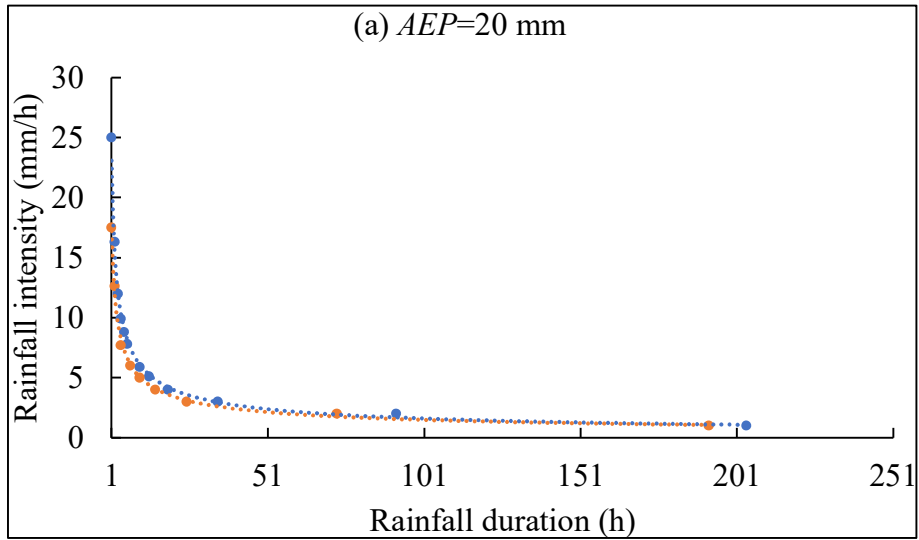
291
292
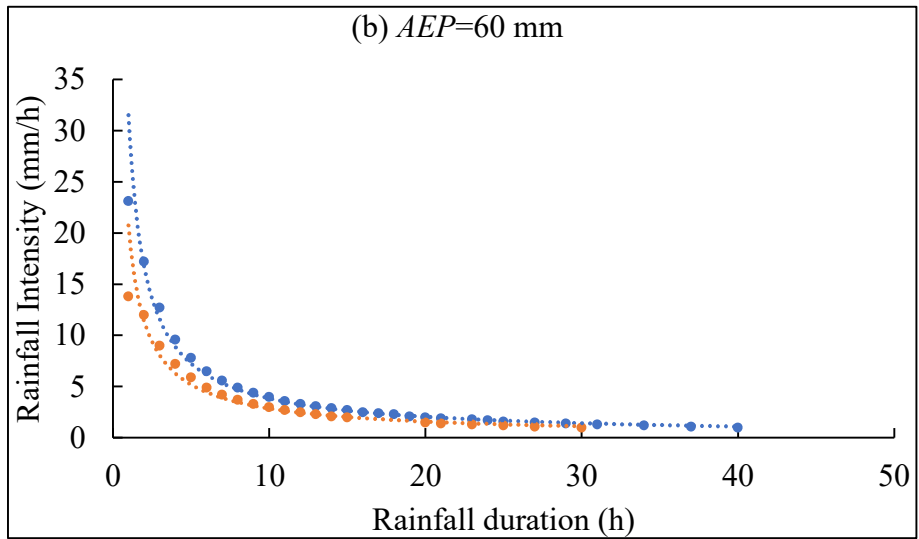
293
294
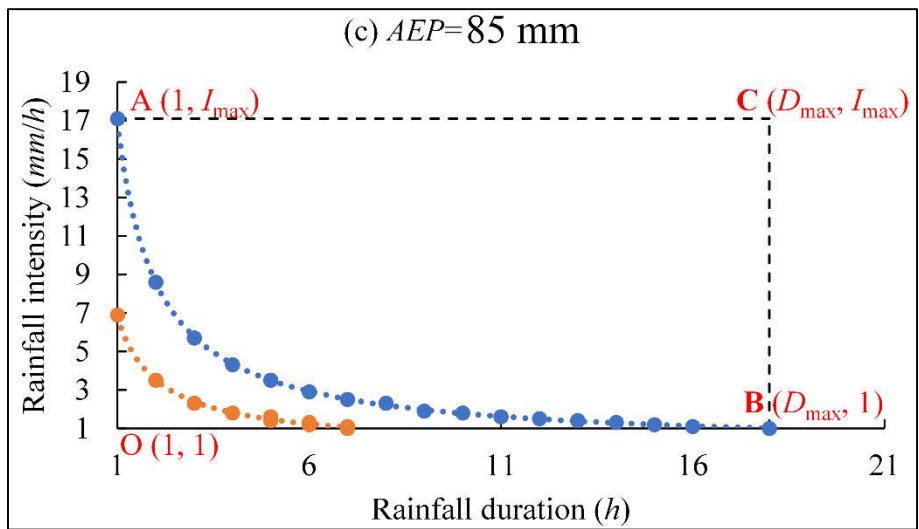
295

296   Fig.2 ID threshold curves derived by Dens-ID (the blue dotted line corresponds to 1.2 g/cm³, and

297   the orange dotted line corresponds to 2.2 g/cm^3)

298   There are two ID threshold curves in each subplot of Fig. 2, which correspond to 1.2 g/cm^3 and

299 2.2 g/cm^3, respectively. Because the debris flow density in JJG varies within a certain range from

300 1.2–2.3 g/cm^3, the two ID threshold curves shown in each subplot can be regarded as the upper and

301 lower boundary lines for determining the occurrence of debris flow (Zhang et al., 2020). Within the

302 ID coordinate system, the two derived curves together with the I- and D-axes delineate a closed area

303 shown in Fig.2c. Any subsequence rainfall represented by the combination of I and D falling into

304 W_{ID} may trigger a debris flow. As shown in each subplot, the threshold curve can be represented by

305 the power function I=αD^β. The variation intervals of the independent (D) and dependent (I) variables

306 of the power function are [1, D_{max}] and [1, I_{max}], respectively, where D_{max} represents the rainfall

307 duration required to trigger debris flow when I= 1 mm/h, and I_{max} represents the rainfall intensity

308 required for debris flow formation for D=1 h. As shown in Fig.2c, independent variable D and

309 dependent variable I can delineate a larger rectangular area (AOBC) in the ID plane than W_{ID}, which

310 is denoted as R_{ID}. The coverage area of R_{ID} is much larger than that of W_{ID} indicating that the

311 proportion of rainfall conditions that can trigger debris flows is low. Therefore, even for AEP=85

312 mm, the occurrence probability of debris flows remains low. As shown in each subplot, each AEP

313 corresponds to a different W_{ID} and R_{ID}, which provides basic data for the quantitative evaluation of

314 the effect of different AEPs on the occurrence probability of debris flows.

315 **4.2 Occurrence probability of debris flow under different AEP**

316   Based on the Monte Carlo method of calculating the definite integral, it is necessary to explore

317 the probability density function of rainfall duration (D) to calculate the occurrence probability of

318 debris flow under different AEP conditions. For the 1094 rainfall events listed in Appendix 1, we

319   found that the probability distribution of rainfall duration D in JJG can be described by a power

320   function (Fig. 3). As shown in Fig.3, the number of samples with D<1 accounted for 37.7%, 1<D<3

321   for 23.5%, 3<D<5 for 14.7%, and 5<D<10 for 16.9%; the number of rainfall events with D

322   exceeding 10 h accounted for only 6.7%.
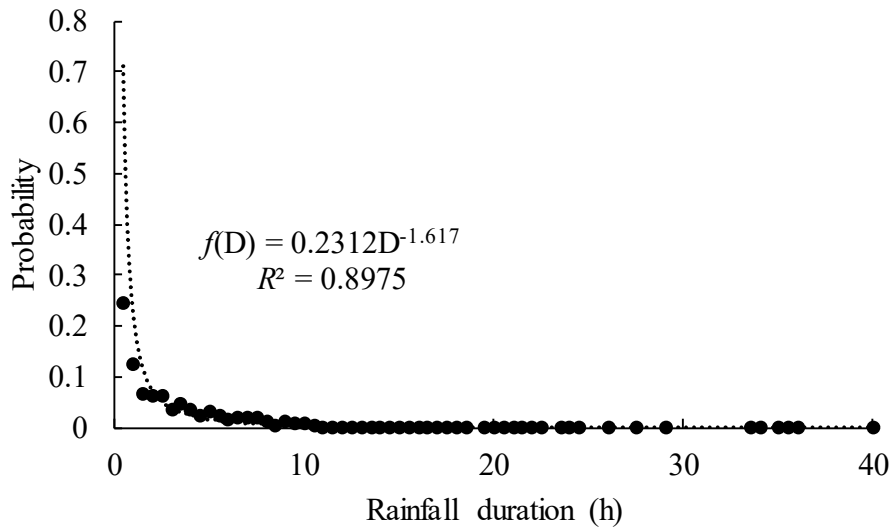
323

324   Fig. 3 Probability density function of f(D)

325   Based on the probability density distribution function f(D)=0.2312D$^{-1.617}$, the cumulative

326   probability function cdf(D) can be obtained through integration. In cdf(D), denoted as Equation 13,

327   the integration constant C needs to be determined.

328 $$cdf(D)= \int_{-\infty}^{D} f(D)dD = -0.3747*D^{-0.617}+C \tag{13}$$

329   The range of 0–40 h is evenly divided into 56 statistical intervals (the second column in

330   Appendix 2, titled "appendix 2-f(D)and CFD(D). xlsx"), and each statistical interval is separated by

331   0.5 h. The proportion of the sample size in each interval among the 1094 samples can be calculated

332   and listed in the second column in Appendix 2; the cumulative proportion that increases with D is

333   also derived and listed in the third column in Appendix 2. The data in the first and third columns of

334   Appendix 2 are substituted into Equation 13 to calculate C. The results show that C increases with

335   D but gradually stabilizes at approximately 1.04 (the fifth column in Appendix 2). Therefore, C is

336   set to 1.04.

337   Based on the process of calculating P_{df} under different AEP conditions in Section 3.4, the P_{df}

338   corresponding to each AEP in Table 1 is obtained, and the function $P_{df} = f(AEP)$ for describing

339   their relationship has been fitted using the AEP and P_{df} data.

340     $$P_{df} = 0.3442e^{0.0457AEP} \tag{14}$$

341   As shown in Equation14, the relationship of AEP and P_{df} obeys the rule of exponential function

342   as AEP changes from 10 to 85 mm, whereas $P_{df} = 0$ when AEP is less than 10 mm. The evolution

343   of P_{df} with AEP variation can be divided into two stages (Fig. 4). Two key issues must be stated

344   before discussing the two stages in depth: (1) Based on the calculation results of the Dens-ID model,

345   an upper limit volume of the rainfall-induced solid material supply is derived in JJG, which is the

346   basic condition for determining the scale of debris flow in JJG (Zhang et al., 2020). (2) Based on

347   the principle of water balance, AEP is defined as the rainfall that is preserved in the soil before the

348   triggering rainfall process (Kohler and Linsley, 1951); field observations in JJG show that the AEP

349   is positively correlated with the soil water content (Cui et al., 2007), and the field observations of

350   the Liudaogou catchment in the northern Loess Plateau of China have the same result (Zhu and

351   Shao, 2008); therefore, the AEP is typically used to estimate soil water content (Crozier, 1986; Chen

352   et al., 2018; Zhao et al., 2019b). The water soil content before the triggering rainfall process can be

353   characterized by AEP (Thomas et al., 2019; Schoener and Stone, 2020).
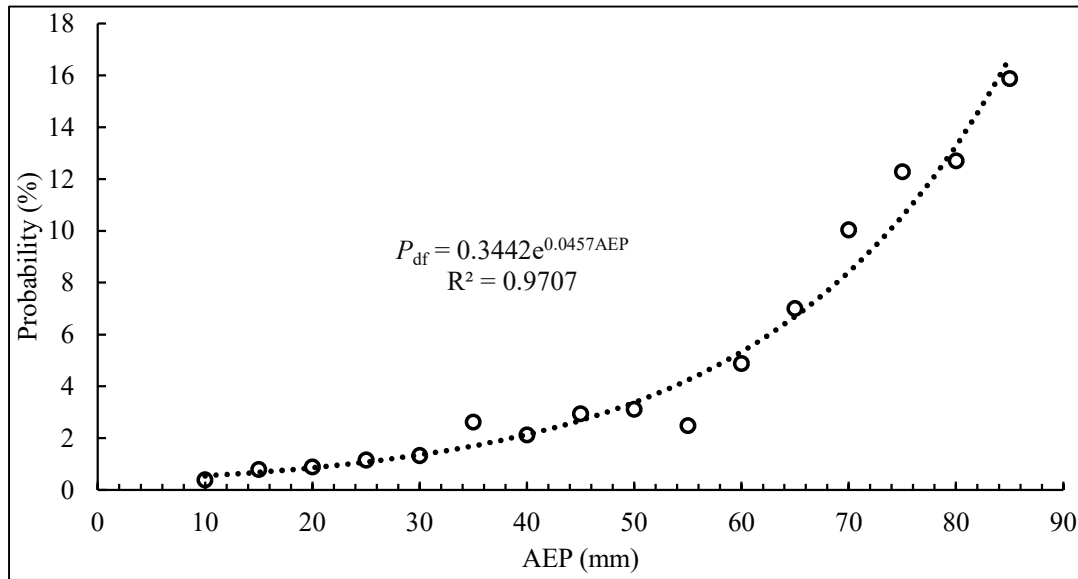
Fig.4 Relationship of P_{df} and AEP derived from Dens-ID

Stage 1: The probability of debris flow occurrence in JJG is equal to 0 when the AEP is < 10

mm. Dens-ID estimates the solid material volume by simulating rainfall-induced shallow landslides.

According to Equation 4, the key hydrological process that triggers shallow landslides is the

continuous increase in soil water content caused by rainfall infiltration. The increase in soil moisture

content reduces soil matrix suction and eventually contributes to shallow landslides. The soil water

content of the loose soil mass in JJG is low when the AEP < 10 mm (Long et al., 2020), and a long

duration of rainfall infiltration is needed to increase the soil water content. However, based on the

infiltration border of Dens-ID (Equation 1), limited by the infiltration capacity of the topsoil in JJG,

the portion of precipitation that exceeds the infiltration capacity is be converted into runoff;

therefore, when the water content of the soil layer in JJG is low, the surface runoff can be rapidly

generated. Therefore, the runoff generation rate can be much higher than the supply rate of solid

material in the condition of AEP < 10 mm. In this hydrological scenario, Dens-ID determines that

even a soil-water mixture with a density of 1.2 g/cm^3 is difficult to generate in JJG; thus, the

probability of debris flow is 0.

Stage 2: When AEP varies within the interval of 10 mm-85mm, the subsequent rainfall is capable of triggering debris flow in JJG. Compared to AEP < 10 mm in Stage 1, the soil water content within JJG increased significantly. Therefore, the solid material from shallow landslides can be immediately ready without a long rainfall infiltration duration, and a large water content of topsoil is beneficial to the rapid generation of runoff (Jones et al., 2017; Hirschberg et al., 2021). When there is a sufficient supply of solid material and runoff, the probability of debris flow occurrence in Stage 2 is significantly increased by the increasing AEP. The relationship between $P_{df} \sim AEP$ can be described by an exponential function of $P_{df}=0.3442e^{0.0457AEP}$. The exponential function and its boundary show that the increasing tendency of P_{df} is a little sluggish before AEP is equal to 50 mm. The occurrence probability of debris flow in JJG is only 15.88% even when AEP is equal to 85 mm.

5 Discussions

5.1 Correlation analysis of the two curves derived from Dens-ID and observation data

The AEP in Appendix 1 varied from 0–87.9 mm, according to this range, we can test the reasonability of the relationship between $P_{df} \sim AEP$ shown in Fig. 4. We introduce how to use the rainfall and debris flow data recorded in Appendix 1 to calculate P_{df}: (1) The original AEP value is rounded to one decimal place, and the rounded AEP are listed in the 8th column of Appendix 1, which were sorted from largest to smallest; (2) the maximum AEP_i was set to 85 mm, and [AEP_i, AEP_i-5] was used as the search window to collect the rainfall events and debris flow events; and (3) we count the number of debris flow events N_{df} and the number of rainfall events N_{rain} in each search window and then calculate $P_{df}=N_{df}/N_{rain}$. Based on the above steps, the collected data and calculated

391   P_{df} are listed in Table 2. As shown in Table 2, a positive correlation between the probability of debris

392   flow occurrence and AEP in JJG was determined. When AEP < 10 mm, a total of 205 rainfall

393   processes were recorded; however, no debris flow events were observed, and the debris flow

394   occurrence probability was 0, which is consistent with the results of Stage 1 derived from Dens-ID.

395   Table 2 Collected and calculated P_{df} in each search window

	Field observation data and calculated P_{df}										
AEP	10	15	20	25	30	35	40	45	50	75	80
N_{df}	0	3	2	7	7	4	4	5	3	1	1
N_{rain}	205	133	111	127	124	106	106	49	31	8	5
P_{df}(%)	0	2.3	1.8	5.5	5.6	3.8	3.8	10.2	9.7	12.5	20

396   Based on P_{df} and AEP listed in Table 2, their relationship can be described by the exponential

397   function denoted as $P_{df} = 1.5917e^{0.031AEP}$, which is similar to Equation14 drawn in Fig.4. The

398   two curves were nearly parallel. Equation 12 was used to analyze the correlation of the two curves,

399   and r is equal to 0.93, suggesting they have a very high correlation. Therefore, the function of $P_{df} =$

400    $f(AEP)$ derived from Dens-ID, which is used to describe the evolution trend of debris flow

401   occurrence probability with AEP variation, is reasonable.
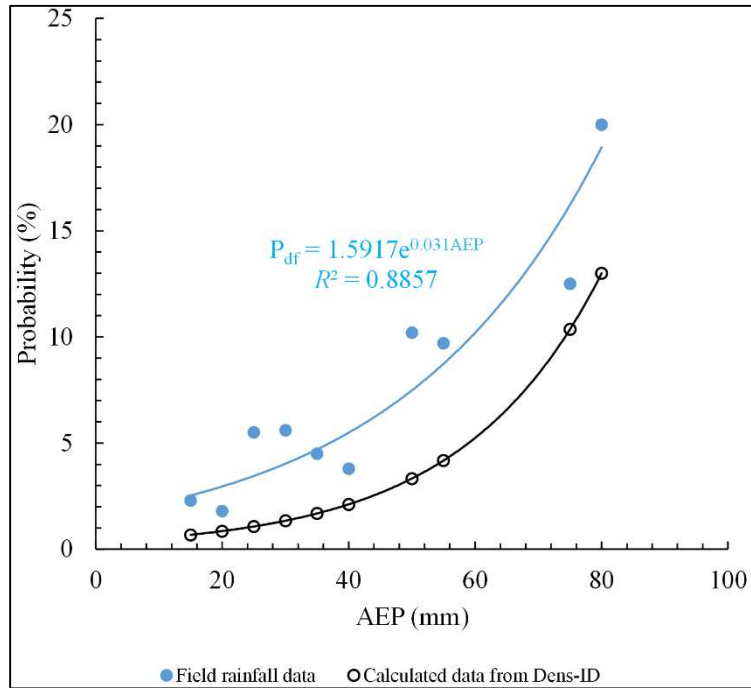
402

403   Fig.5 Relationship of AEP and P_{df} obtained from field observation data and Dens-ID model (the blue line is

404   derived from field observation data, and the black line is derived from Dens-ID)

405   We can also see from Fig.5 that although the variation tendencies of the two curves are

406   consistent, a significant bias existed between them. Basically, the probability value derived from the

407   field observation data is larger than that from the Dens-ID model in the condition of a given AEP.

408   As shown in Fig.5, the blue line fitted through the observation data is above the black line derived

409   from Dens-ID, indicating that Dens-ID underestimated the probability of debris flow occurrence if

410   the observation data were used as the reference. Taking the probability value in the 6th row of Table

411   2 as references, the error of the Equation14 was calculated using the AEP in Table 2 as inputs and

412   listed in Table 3.

413   Table 3 Error estimation on the Equation 14

AEP	15	20	25	30	35	40	45	50	75	80
Error	0.70	0.53	0.81	0.76	0.63	0.44	0.67	0.57	0.17	0.35

414   It can be seen that very large bias of Equation12 is listed in Table 2. However, we cannot

415   conclude that there is a precision problem in the calculation results of the Dens-ID. Because (1)

416   Although 1094 rainfall processes and 37 debris flow events are the field observation data, there are

417   many uncertain factors in Equation 7 for calculating AEP using these rainfall data (Kim et al., 2021),

418   such as the subjectivity existing in K and n of Equation 7, which render uncertainty in the calculated

419   AEP. In this case, if the data in Appendix 1 are used as the real value for evaluating the precision of

420   Dens-ID, the error evaluation result may be unfair to Dens-ID. In this case, it is unfair to evaluate

421   the Dens-ID error by using the calculated AEP in Appendix 1 as the true value. However, this

422   uncertainty can show consistent directional deviations because of the fixed values of K and n in

423   Equation 7; therefore, the uncertainty has no effect on the correlation analysis. (2) To establish the

424   functional relationship between P_{df}-AEP, many rainfall scenarios were simulated using the Dens-ID

425   model. Dens-ID simulated 3376, 3182, 2677, and 2677 rainfall processes with AEP = 20, 40, 45,

426   and 50 mm, respectively. The total number of simulated rainfall processes was significantly larger

427   than that of the 1094 observed rainfall events. The collected 1094 rainfall events still cannot fully

428   reflect all rainfall conditions in nature; that is, the amount of the observed 1094 rainfall data is still

429   inadequate when used as the denominator for calculating the probability of debris flow occurrence

430   in JJG. Therefore, the P_{df} calculated using the field observation data may be generally higher than

431   that calculated using Dens-ID. With the accumulation of rainfall observation data of JJG, it is

432   believed that the Pdf derived from field observation data will gradually decrease until it is close to

433   the calculated value of Dens-ID model. (3) Dens-ID cannot fully and accurately describe the

434   formation process of the debris flow in JJG because of the simplification in theory and boundaries.

435   Dens-ID is also affected by the accuracy of the input parameters (Zhang et al., 2020), which may

436   eventually lead to deviations between the simulation results and field observations.

437   5.2 Potential application and limitation

438   Deriving a quantified functional relationship of P_{df} and AEP would be more conducive to

439   examining the correspondence between these two parameters. Using mathematical physics method,

440   the function of $P_{df} = f(AEP)$ was firstly derived which can help us to learn more from the derived

441    $P_{df} = f(AEP)$.

442   Firstly, AEP is indeed an important factor affecting debris flow. Generally, there is the

443   following consensus in the field of debris flow: the greater the AEP, the higher the probability (P_{df})

444   of subsequent rainfall triggering the debris flow (De Vita et al., 2000; Bel et al., 2017). However,

445   this fuzzy qualitative description cannot explain the influence degree of AEP on the probability of

446   debris flow induced by subsequent rainfall. It can be seen from $P_{df} = f(AEP)$ that there are two

447   key value nodes of AEP affecting P_{df}: (1) point 10 mm:the case of AEP < 10 mm indicates that

448   any subsequent rainfall cannot trigger debris flow in JJG. Because the supply rate of solid material

449   is much lower than the runoff generation rate during subsequent rainfall in JJG, the water-soil

450   mixture within tends to be a hyperconcentrated flow rather than a debris flow (Long et al., 2020);

451   (2) Point 50 mm: the case of 10 mm≤AEP≤50 mm means that the soil water content increases

452   significantly compared to AEP < 10 mm, but a necessary infiltration time to increase it to the critical

453   state for triggering shallow landslides is still required. Therefore, limited by the supply rate of the

454   solid material, the increasing rate of P_{df} is sluggish. The case of 50 mm<AEP≤85 mm represents

455   the soil water content is relatively larger, the solid material from shallow landslides can be

456   immediately ready without a long rainfall infiltration duration, and a large soil water content of

457   topsoil is beneficial to the rapid generation of runoff (Jones et al., 2017; Hirschberg et al., 2021).

458   When there is a sufficient supply of provenance and runoff, the probability of debris flow occurrence

459   in this subprocess is significantly enhanced by the increasing AEP.

460   Secondly, Rainfall-induced debris flow is a small probability event compared with the rainfall

461   frequency in nature. JJG is well-known due to its high-frequency debris flow event. However, the

462   formation probability of debris flow in JJG induced by subsequence rainfall is only 15.88% even

463   the AEP reaches to 85 mm. Therefore, debris flow induced by rainfall in JJG is a small probability

464   event compared with the rainfall frequency. The figure of 15.88% means that the efficiency of rain-

465   induced debris flow is extremely low, which also indicates that the formation of debris flow is an

466   extremely complex physical process, in which rainfall is only one of the motivating factors, and

467   there are other more important internal factors affecting the formation of debris flow, such as

468   topography, source recharge and fluid characteristics of debris flow (Zhang et al., 2020). Thirdly, in

469   practical application, when the AEP in JJG is calculated according to Equation 7, the derived

470   exponential function can help us to assess the probability of debris flow in JJG triggered by

471   subsequent rainfall, according to which debris flow warning information can be issued in advance

472   to provide technical support for disaster prevention and reduction.

473   Our study also has its own limitations and needs to be listed for providing directions for

474   subsequent investigation. (1) Long-term observation data should be used to deduce the functions of

475    $P_{df} = f(AEP)$, however, the number of debris flow gullies with long-term observational data

476   worldwide is less than 10 (Hürlimann et al., 2019), accordingly, the function of $P_{df} = f(AEP)$

477   cannot yet be derived in other debris-flow gullies. (2) Dens-ID model assumes that the solid

478   material mainly comes from shallow landslides. However, the formation mechanism and solid

479   source supply mode of runoff-induced debris flow are different. Therefore, the functional of $P_{df} =$

480    $f(AEP)$ for runoff-induced debris flow still needs to be studied with the help of other physical

481 models. (3) The calculation result of $P_{df} = f(AEP)$ derived from Dens-ID model has a large bias

482 from the observation data, the authors think that the main reason is insufficient field observation

483 data especially inadequate rainfall data. Basically, even for high-frequency debris flow gullies like

484 JJG, the success rate of debris flow induced by rainfall is still very low. Continuous increase of

485 rainfall and debris flow observation data will make the growth rate of Nrain in Table 2 much higher

486 than that of Ndf. Therefore, with the accumulation of rainfall observation data of JJG, it is believed

487 that the P_{df} derived from field observation data will gradually decrease until it is close to the

488 calculated result of Dens-ID model. Therefore, the authors will continue to collect field observation

489 data of JJG in the later period, and constantly verify the accuracy of Equation14 derived from Dens-

490 ID.

491 **5 Conclusions**

492 The Dens-ID model and Monte Carlo integral equation is used to derive function of $P_{df} =$

493 $f(AEP)$. The functional relationship is verified using a large amount of field observation data from

494 JJG. The following conclusions are drawn as follows.

495 The positive relationship between P_{df} and AEP is now described by a clear mathematical

496 equation in this study. the effective range of AEP that can affect debris flow formation verifies within

497 10–85 mm. Based on the simulation results, the probability of debris flow occurrence in JJG is 0 in

498 the condition of AEP < 10 mm, and the relationship between P_{df} and AEP can be described by an

499 exponential function when 10 mm≤AEP≤85 mm. The plausibility of the first two evolution stages

500 of the P_{df}-AEP piecewise function is effectively confirmed by the field observation data because the

501 P_{df}-AEP relationship obtained from field observation data is highly correlated with the simulation

502 results of Dens-ID. However, the reasonability of the last two stages of the P_{df}-AEP piecewise

function cannot be tested because of the lack of field observation data, and the errors of the P_{df}-AEP

piecewise function cannot be verified because of the uncertainty of the AEP derived from the

observation rainfall data.

This study mathematically confirms that "the greater the AEP, the higher the probability of

subsequent rainfall triggering debris flow" and quantifies this qualitative conclusion using piecewise

functions. This can effectively reveal the essential relationship between the two natural events of

rainfall and debris flow, quantitatively describe the impact of different AEPs on the probability of

debris flow occurrence, and provide key technical support for the early warning of debris flows.

Acknowledgement:

This work was supported by the National Key Research and Development Program of China

(2023YFC3007205), the West Light Foundation of The Chinese Academy of Science, National

Natural Science Foundation of China (No. 42271013, No. 42001100), Project of the Department of

Science and Technology of Sichuan Province (No. 2023ZHCG0012).

References

Abraham, M.T., Satyan, N., Rosi, A., Pradhan, B., Segoni, S.: Usage of antecedent soil moisture for

    improving the performance of rainfall thresholds for landslide early warning. Catena, 200,

    105147, 2021.

Abraham, M.T., Satyam, N., Pradhan, B., Alamri, A.M.: Forecasting of landslides using rainfall

    severity and soil wetness: A probabilistic approach for Darjeeling Himalayas. Water (Switzerland)

    12, 1–19, 2020.

Adams, B., Fraser, H., Howard, C., Hanafy, M.: Meteorological data analysis for drainage system

    design. J. Environ. Eng. 112, 1986.

525   Albert, G.E.: A general theory of stochastic estimates of the Neumann series for solution of certain

526   Fredholm integral equations and related series, in: M.A. Meyer (Ed.), Symposium of Monte Carlo

527   Methods, Wiley, New York, 1956.

528   Bel, C., Liébault, F., Navratil O., Eckert N., Bellot H., Fontaine, F., Laigle, D.: Rainfall control of

529   debris-flow triggering in the Réal Torrent, Southern French Prealphs, 291, 17-32, 2017.

530   Bennett, G.L., Molnar, P., Mcardell, B.W., Burlando, P.: A probabilistic sediment cascade model of

531   sediment transfer in the Illgraben. Water Resources Research, 50, 1225-1244, 2014.

532   Bernard, M., Gregoretti, C.: The use of rain gauge measurements and radar data for the model-based

533   prediction of runoff-generated debris flow occurrence in early warning systems. Water Resources

534   Research, 57, e2020WR027893, 2021.

535   Berti, M., Simoni, A.: Experimental evidences and numerical modelling of debris flow initiated by

536   channel runoff. Landslides, 3, 171-182, 2005.

537   Calvo, B., Savi, F.: A real-world application of Monte Carlo procedure for debris flow risk

538   assessment, Computers and Geosciences, 35(5), 967-977, 2009.

539   Castillo, V.M., Gómez-Plaza, A., Martínez-Mena, M.: The role of antecedent soil water content in

540   the runoff response of semiarid catchments: a simulation approach. Journal of Hydrology, 284,

541   114-130, 2003.

542   Chen, C.W., Oguchi, T., Chen, H., Lin, G.W. Estimation of the antecedent rainfall period for mass

543   movements in Taiwan, Environmental Earth Sciences, 77, 184, 2018.

544   Chen, C.W., Saito, H., Oguchi, T.: Analyzing rainfall-induced mass movements in Taiwan using the

545   soil water index, Landslides, 14, 1031-1041, 2017.

546   Coe, J.A., Kinner, D.A., Godt, J.W. Initiation conditions for debris flows generated by runoff at

547   Chalk Cliffs, central Colorado. Geomorphology, 3, 270-297, 2008.

548   Crozier, M.J.: Landslides: causes, consequences & environment. Croom Helm, London, p 25, 1986.

549   Cui, P., Zhu, Y.Y., Chen, J., Han, Y.S., Liu, H.J.: Relationships between antecedent rainfall and

550   debris flows in Jiangjia Ravine, China. In: Chen & Major, eds., Debris-Flow Hazards Mitigation:

551   Mechanics, Prediction, and Assessment, Millpress, Netherlands, 3-10, 2007.

552   De Vita, P.: Fenomeni d'instabilita` delle coperture piroclastiche dei Monti Lattari, di Sarno e di

553   Salerno (Campania) ed analisi degli eventi pluviometrici determinanti. Quad. Geol. Appl., 7, 213–

554   239, 2000.

555   Donovan, I.P., Santi, P.M. A probabilistic approach to post-wildfire debris-flow volume modeling,

556   Landslides, 14(4): 1345-1360, 2017.

557   Fiorillo, F., Wilson, R.C. Rainfall induced debris flows in pyroclastic deposits, Campania (southern

558   Italy). Engineering Geology, 75, 263-289, 2004.

559   Gabet, E.J., Mudd, S.M.: The mobilization of debris flows from shallow landslides. Geomorphology

560   1, 207-218, 2006.

561   Han, Z., Chen, G.Q., Li, Y.G., He, Y.: Assessing entrainment of bed material in a debris-flow event:

562   a theoretical approach incorporating Monte Carlo method: Assessing Entrainment of Bed

563   Material by Debris Flow, Earth surface processes and landforms, 40(14): 1877-1890, 2015.

564   Hirschberg, J., Badoux, A., McArdell, B.W., Leonarduzzi, E., Molnar, P.: Evaluating methods for

565   debris-flow prediction based on rainfall in an Alpine catchment. Nat. Hazards Earth Syst. Sci.,

566   21, 2773-2789, 2021.

567   Hong, M., Kim, J., Jeong, S.: Rainfall intensity-duration thresholds for landslide prediction in South

568   Korea by considering the effects of antecedent rainfall. Landslides, 15, 523–534, 2018.

569   Hu, W., Xu, Q., Wang, G.H., van Asch, T.W.J., Hicher, P.Y.: Sensitivity of the initiation of debris

570   flow to initial soil moisture. Landslides 12, 1139–1145, 2015.

571   Huang, C.H.: Critical rainfall for typhoon-induced debris flows in the Western Foothills, Taiwan.

572   Geomorphology, 185, 87-95, 2013.

573   Hürlimann, M. Coviello, V., Bel, C., Guo, X.J., Berti, M., Graf, C., Hübl, J., Miyata, S., Smith, J.B.,

574   Yin, H.Y.: Debris-flow monitoring and warning, Review and examples. Earth-Science Reviews,

575   199, 102981, 2019.

576   Iverson, R. M., Reid, M. E., LaHusen, R. G.: Debris Flow Mobilization from Landslides. Annu. Rev.

577   Earth Planet, 25: 85-138, 1997.

578   Jones, R., Thomas, R.E., Peakall, J., Manville, V.: Rainfall-runoff properties of tephra: Simulated

579   effects of grain-size and antecedent rainfall. Geomorphology, 282, 39-51, 2017.

580   Kim, S.W., Chun, K.W., Kim, M., Catani, F., Choi, B., Seo, J.: Effect of antecedent rainfall

581   conditions and their variations on shallow landslide-triggering rainfall thresholds in South Korea.

582   Landslides, 18, 569-582, 2021.

583   Kohler, M.A., Linsley, R.K.: Predicting the runoff from Storm Rainfall. US Department of

584   Commerce, Weather Bureau, Washington, D.C, 1951.

585   Le Bissonnais, Y., Renaux, B., Delouche, H. Interactions between soil properties and moisture

586   content in crust formation, runoff and interrill erosion from tilled loess soils. Catena, 25(1), 33-

587   46, 1995.

588   Li, L., Zhang, S.X., Li, S.H., Qiang, Y., Zheng, Z., Zhao, D.S.: Debris Flow Risk Assessment

589   Method Based on Combination Weight of Probability Analysis, Advances in civil engineering,

590   2021, 1-12, 2021.

591 Liu, D.L., Zhang, S.J., Yang, H.J., Zhao, L.Q., Jiang, Y.H., Tang, D., Leng, X.P.: Application and

592   analysis of debris-flow early warning system in Wenchuan earthquake-affected area. Nat. Hazards

593   Earth Syst. Sci., 16, 483-496, 2016.

594 Liu, X.L., Wang, F., Nawnit, K., Lv, X.F., Wang, S.J. Experimental study on debris flow initiation.

595   Bulletin of Engineering Geology and the Environment, 79, 1565-1580, 2020.

596 Long, K., Zhang, S.J., Wei, F.Q., Hu, K.H., Zhang, Q., Luo, Y. A hydrology-process based method

597   for correlating debris flow density to rainfall parameter and its application on debris flow

598   prediction. Journal of Hydrology, 589, 125124, 2020.

599 Luk, S.H.: Effect of antecedent soil moisture content on rainwash erosion. Catena, 12, 129-139,

600   1985.

601 Marra, F., Destro, E., Nikolopoulos, E.I., Zoccatelli, D., Creutin, J.D., Guzzetti, F., Borga, M.:

602   Impact of rainfall spatial aggregation on the identification of debris flow occurrence thresholds.

603   Hydrol. Earth Syst. Sci., 21, 4525-4532, 2017.

604 Paola, F.De., Risi, R.De., Crescenzo, G. Di, Giugni, M., Santo, A., Speranza, G.: Probabilistic

605   Assessment of Debris Flow Peak Discharge by Monte Carlo Simulation, Journal of Risk and

606   Uncertainty in Engineering Systems, Part A: Civil Engineering, 3(1), A4015002, 2017.

607 Papa, M.N., Medina, V., Ciervo, F., Bateman, A.: Derivation of critical rainfall thresholds for

608   shallow landslides as a tool for debris flow early warning systems. Hydrol. Earth Syst. Sci. 17,

609   4095-4107, 2013.

610 Peres, D.J., Cancelliere, A.: Derivation and evaluation of landslide-triggering thresholds by a Monte

611   Carlo approach. Hydrol. Earth Syst. Sci., 18, 4913-4931, 2014.

612 Peres, D.J., Cancelliere, A.: Modeling impacts of climate change on return period of landslide

triggering. Journal of Hydrology, 567, 420-434, 2018.

Richards, L.A. Capillary condition of liquids in porous mediums. Physics 1, 318–333, 1931.

Schoener, G., Stone, M.C.: Monitoring soil moisture at the catchment scale-A novel approach combing antecedent precipitation index and rader-derived rainfall data, Journal of Hydrology, 589, 125155, 2020.

Segoni, S., Piciullo, L., Gariano, S.L.: A review of the recent literature on rainfall thresholds for landslide occurrence, Landslides, 15:1483-1501, 2018b.

Segoni, S., Rosi, A., Lagomarsino, D., Fanti, R., Casagli, N.: Brief communication: Using averaged soil moisture estimates to improve the performances of a regionalscale landslide early warning system. Nat. Hazards Earth Syst. Sci. 18, 807–812, 2018a.

Senthilkumar, V., Chandrasekaran, S.S., Maji, V.B.: Geotechnical characterization and analysis of rainfall-induced 2009 landslide at Marappalam area of Nilgiris district, Tamil Nadu state, India. Landslides, 14, 1803-1814, 2017.

Tang, H., Mcguire, L.A., Kean, J.W., Smith, J.B.: The impact of sediment supply on the initiation and magnitude of runoff-generated debris flows. Geophysical Research Letters, 47, e2020GL087643, 2020.

Thomas, M.A., Collins, B.D., Mirus, B.B.: Assessing the feasibility of satellite-based thresholds for hydrologically driven landsliding. Water Resource Research, 55, 9006-9023, 2019.

Tisdall, A.: Antecedent soil moisture and its relation to infiltration. Aust. J. Agric. Res., 2 (3), 342–348, 1951.

Van Genuchten, M.: A closed form equation for predicting the hydraulic conductivity of unsaturated soils. Soil Sci. Soc. Am. J. 44, 892–898, 1980.

635 Wei, F.Q., Hu, K.H., Zhang, J., Jiang, Y.H., Chen, J.: Determination of effective antecedent rainfall

636   for debris flow forecast based on soil moisture content observation in Jiangjia Gully, China. In:

637   DeWrachien, D., Brebbia, C.A., Lenzi, M.A., eds., Monitoring, Simulation, Prevention and

638   Remediation of dense debris flows II. WIT Transactions on Engineering Sciences, England. 13-

639   22, 2008.

640 Yan, Z.Z., Hong, Z.M.: Using the Monte Carlo method to solve integral equations using a modified

641   control variate. Applied mathematics and computation, 242,764-777, 2014.

642 Yang, H.J., Zhang, S.J., Hu, K.H., Wei, F.Q., Wang, K., Liu S.: Field observation of debris flow

643   activities in the initiation area of Jiangjia Gully, Yunnan Province, China, Journal of Mountain

644   Science, 19(6): 1602-1617, 2022.

645 Zeng, Q.L., Yue, Z.Q., Yang, Z.F., Zhang, X.J.: A case study of long-term field performance of

646   check-dams in mitigation of soil erosion in Jiangjia stream, China. Environ Geol 58:897–911,

647   2009.

648 Zhang, S.J., Xu, C.X., Wei, F.Q., Hu, K.H., Xu, H., Zhao, L.Q., Zhang, G.P.: A physics-based model

649   to derive rainfall intensity-duration threshold for debris flow. Geomorphology, 351, 106930, 2020.

650 Zhang, S.J., Yang, H.J., Wei, F.Q., Jiang, Y.H., Liu, D.L.: A model of debris flow forecast based on

651   the water-soil coupling mechanism. Journal of Mountain Science, 25, 757-763, 2014.

652 Zhang, S.J., Xia, M.Y., Li, L., Yang, H.J., Liu, D.L., Wei, F.Q.: Quantify the effect of antecedent

653   effective precipitation on rainfall intensity-duration threshold of debris flow. Landslides, 20,

654   1719-1730, 2023.

655 Zhao, B.R., Dai, Q., Han, D.W., Dai, H.C., Mao, J.Q., Zhuo, L.: Probabilistic thresholds for

656   landslides warning by integrating soil moisture conditions with rainfall thresholds. Journal of

657   Hydrology, 574, 276-287, 2019a.

658   Zhao, B.R., Dai, Q., Han, D., Dai, H., Mao, J., Zhuo, L., Rong, G.: Estimation of soil moisture using

659   modified antecedent precipitation index with application in landslide predictions. Landslides 16,

660   2381–2393, 2019b.

661   Zhu, Y.J., Shao, M.G.: Variability and pattern of surface moisture on a small-scale hillslope in

662   Liudaogou catchment on the northern Loess Plateau of China, Geoderma, 147, 185-191, 2008.

663   Zhuang, J.Q., Cui, P., Wang, G.H., Chen, X.Q., Iqbal, J., Guo, X.J.: Rainfall thresholds for the

664   occurrence of debris flows in Jiangjia Gully, Yunnan Province, China. Eng. Geol. 195, 335–346,

665   2015.